Spatial and Temporal Distribution of Latent Heating in the South Asian Monsoon Region

MANUEL D. ZULUAGA, CARLOS D. HOYOS, AND PETER J. WEBSTER

School of Earth and Atmospheric Sciences, Georgia Institute of Technology, Atlanta, Georgia

(Manuscript received 9 January 2009, in final form 5 October 2009)

ABSTRACT

Information from the Tropical Rainfall Measuring Mission (TRMM) level 3 monthly 0.5° × 0.5° Convective and Stratiform Heating (CSH) product and TRMM Microwave Imager (TMI) 2A12 datasets is used to examine the four-dimensional latent heating (LH) structure over the Asian monsoon region between 1998 and 2006. High sea surface temperatures, ocean–land contrasts, and complex terrain produce large precipitation and atmospheric heating rates whose spatial and temporal characteristics are relatively undocumented. Analyses show interannual and intraseasonal LH variations with a large fraction of the interannual variability induced by internal intraseasonal variability. Also, the analyses identify a spatial dipole of LH anomalies between the equatorial Indian Ocean and the Bay of Bengal regions occurring during the summer active and suppressed phases of the monsoon intraseasonal oscillation. Comparisons made between the TRMM CSH and TMI 2A12 datasets indicate differences in the shape of the vertical profile of LH. A comparison of TRMM LH retrievals with sounding budget observations made during the South China Sea Monsoon Experiment shows a high correspondence in the timing of positive LH episodes during the rainy periods. Negative values of atmospheric heating, associated with radiative cooling and with upper-tropospheric cooling from nonsurface-precipitating clouds, are not captured by either of the TRMM datasets. In summary, LH algorithms based on satellite information are capable of representing the spatial and temporal characteristics of the vertically integrated heating in the Asian monsoon region. However, the vertical distribution of atmospheric heating is not captured accurately throughout different convective phases. It is suggested that satellite-derived radiative heating/cooling products are needed to supplement the LH products in order to give a better overall depiction of atmospheric heating.

1. Introduction

The release of latent heat in the tropical atmosphere accounts for approximately 75% of the total heating in the earth's atmosphere (e.g., Riehl and Malkus 1958; Malkus 1962; Riehl and Simpson 1979). Tropical latent heating (LH) plays a major role in driving and modulating tropical and extratropical weather across all spatial and temporal scales from meso- and synoptic to planetary scales (e.g., Matsuno 1966; Webster 1972; Gill 1980; Hartmann et al. 1984; Mapes 1993; Nigam et al. 2000). LH in precipitating systems is also associated with vertical energy transport throughout the troposphere (Houze 1982). As a consequence, determination of the horizontal and vertical distribution of LH provides a basis for understanding the steady- and transient-state structure of the tropics. However, there is a critical limitation: the vertical distribution of LH is not well known.

The dynamical response of the tropical atmosphere depends strongly on both the vertical and horizontal distribution of LH (e.g., Hartmann et al. 1984; DeMaria 1985; Lau and Peng 1987; Nakazawa 1988; Sui and Lau 1989; Emanuel et al. 1994; Yanai et al. 2000; Chiang et al. 2001). These studies show that improved vertical distributions of LH allow a better representation of tropical east–west circulations (e.g., the Walker circulation) by models other than those using simple heating functions, such as Webster (1972) and Gill (1980). However, even the more advanced studies assume spatially and temporally uniform vertical heating profiles, even though it has been demonstrated that the structure of heating in precipitating cloud systems is highly variable (Houze 1982). For example, Schumacher et al. (2004) show that

Corresponding author address: Manuel D. Zuluaga, 311 Ferst Drive, School of Earth and Atmospheric Sciences, Georgia Institute of Technology, Atlanta, GA, 30332.
E-mail: mzuluaga@gatech.edu

DOI: 10.1175/2009JCLI3026.1

geographical and temporal variability in convective and stratiform rain fractions, both of which have different vertical heating distributions, plays an important role in shaping the structure of the large-scale tropical circulation response, stressing the importance of accurate estimates of the temporal and three-dimensional variability of LH.

In general, it is difficult to determine the vertical distribution of LH because it is not directly measurable and is, by necessity, a derived product. Furthermore, there is a general lack of high-resolution thermodynamic cloud structure information, which would be required to derive LH profiles over long periods of time and large spatial scales. LH variability is particularly high in the South Asian monsoon region (SAMR), where there is a conjunction of high sea surface temperature (SST) and the largest precipitation rates on the planet. In addition, the heating in the monsoon regions has an important influence on the global circulation through the generation of strong teleconnection patterns (Webster 1994; Webster et al. 1998). The SAMR is therefore chosen as the focus of the analysis for these reasons. The specific goal of this study is to examine the four-dimensional structure of LH over the monsoon region for the 1998–2006 period, using the Tropical Rainfall Measurement Mission (TRMM) satellite-based data described in section 2.

An important large-scale feature of the monsoon system is the clustering of synoptic disturbances in periods lasting from 10 to 30 days, resulting in episodes of heavy rainfall and, conversely, periods of limited precipitation. These are referred to as ''active'' and ''break'' periods of the monsoon, respectively (e.g., Krishnamurti and Bhalme 1976; Yasunari 1979; Sikka and Gadgil 1980). Different studies have shown that this intraseasonal variability (20–80 days) of precipitation in the South Asian monsoon is the most important source of weather variability in the region (e.g., Yasunari 1979; Webster et al. 1998; Lawrence and Webster 2002; Webster and Hoyos 2004) with amplitudes greater than the interannual variability and, in some regions, nearly as large as the annual cycle itself (Hoyos and Webster 2007). From a physical perspective, our analysis focuses on exploring differences in the distribution of LH on time scales ranging from interannual to intraseasonal. This study also serves a technological purpose: the determination of the validity the TRMM Level 3 Monthly 0.5° × 0.5° Convective and Stratiform Heating (CSH) and TRMM Microwave Imager (TMI) 2A12 datasets in representing the characteristics of monsoon atmospheric heating.

The paper is organized in the following manner: Section 2 presents brief descriptions of the data. Section 3 describes the spatial and temporal variability of LH for the SAMR, including comparisons between the TRMM CSH and TMI 2A12 datasets. Section 4 presents a validation of the satellite-based LH estimates using independent field campaign data. Section 5 provides an overall summary and lists a number of conclusions.

2. Data

LH estimates used in this study are derived from a combination of TRMM satellite retrievals and cloud-resolving model (CRM) simulations (e.g., Kummerow et al. 1998; Tao et al. 2006). In particular, the TMI and the TRMM Precipitation Radar (PR), which have been providing the distribution of rainfall characteristics throughout the tropics since 1997, are the basis for two different LH datasets: the TRMM CSH and TMI 2A12. These two datasets arise from two independent algorithms: the convective and stratiform heating (CSH; Tao et al. 1993) and the Goddard profiling (GPROF) heating (Olson et al. 1999, 2006), respectively. The relationships between LH and the vertical distribution of hydrometeors, surface rainfall, and the dynamics of mass exchange among cloud layers form the basis of these algorithms.

To obtain estimates of LH over tropical regions, the CSH algorithm uses surface precipitation rates, the percentage of its stratiform and convective components, and the location of the observed cloud system. The foundation of the algorithm is a lookup table (LUT) database of LH profiles based on simulations using the Goddard Cumulus Ensemble (GCE) model and diagnostic heating budgets (Tao and Simpson 1993; Tao et al. 2001). The input source for rainfall information for the CSH algorithm in this study is based on PR rainfall retrievals, in particular, from the 3G68 TRMM product, which also contains cloud classification information from the 2A23 TMI product. The CSH algorithm estimates atmospheric heating [i.e., basically the apparent heat source, Q1; see Tao et al. (2001) for details] for rainy areas only. The data are available for the entire tropical band between 37°S and 37°N at 19 vertical levels from the surface to a height of 18 km with a 0.5° × 0.5° horizontal resolution at daily and monthly resolution. Base LUT profiles representing the vertical heating structure of convective, stratiform, and shallow precipitating systems over land and ocean were used to derive the CSH data in this study. CSH data using these base LUT profiles have been directly compared to observed heating estimates (S. Lang 2008, personal communication). CSH LH estimates had been previously evaluated using in situ data [e.g., Tropical Ocean and Global Atmosphere Coupled Ocean–Atmosphere Response Experiment (TOGA COARE) and ship-based radar] and were reported to be of good quality for different regions of the tropics (Tao et al. 2000, 2001). The main shortcoming of the CSH algorithm is associated with its dependency on

surface rainfall. In the absence of surface rainfall (e.g., nonsurface-precipitating anvils/young convection), the CSH algorithm does not produce estimates of heating. However, on a large-scale view the net amount of LH in the absence of surface precipitation is very small.

The second dataset is derived using a Bayesian approach with a database of hydrometeor profiles and their computed brightness temperatures (Olson et al. 1999). In the algorithm, GCE simulations, coupled to a radiative transfer code, are used to generate a large supporting database of simulated precipitation/LH profiles and corresponding upwelling microwave radiances. For a given set of observed microwave radiances, the entire database of simulated radiances is scanned. The ''retrieved'' profile is a composite of those profiles in the simulated database that are consistent with the observed radiances (Olson et al. 2006). This product provides information on LH over the ocean from the surface to a height of 16 km at 14 vertical levels. The horizontal resolution is about 4.4 km $\times$ 4.4 km over a 759-km-wide swath at an instantaneous time resolution for data before August 2001. After that date, the satellite was moved to a higher orbit decreasing the horizontal resolution to 5.0 km $\times$ 5.0 km over an 858-km-wide swath. Reasonable performance has been reported for LH estimates from the TMI 2A12 V6 algorithm (Tao et al. 2001; Yang et al. 2006).

It is important to note that because the LH estimates from the TMI 2A12 dataset are only available over the ocean, the main analyses in this study are based on the TRMM CSH dataset while the TMI 2A12 dataset is used for comparison. TMI 2A12 data for the summer seasons of the 1998–2006 period, between May and September, were acquired through the Goddard Earth Sciences Distributed Active Archive Center (GES DAAC; online at http://disc.sci.gsfc.nasa.gov/). The TRMM CSH datasets were obtained from two sources: the GES DAAC system (monthly resolution dataset from 1998 to 2006) and directly from W. K. Tao's group in National Aeronautics and Space Administration's (NASA's) Mesoscale Atmospheric Processes Branch (daily dataset for the 1998–2006 period).

Observations obtained during the South Sea China Monsoon Experiment (SCSMEX) conducted from 1 May to 30 June 1998 (Lau et al. 2000) are used to validate the satellite LH estimates for monsoon environments. SCSMEX has two intensive observing networks: one over the northern section of the South China Sea [the northern enhanced sounding array (NESA)] and the other over the southern section of the South China Sea [the southern enhanced sounding array (SESA)], as depicted in Fig. 1 of Johnson and Ciesielski (2002). Multiple SCSMEX observation platforms (e.g., atmospheric soundings, Doppler radar, ships and wind profilers) were deployed to document changes in convection and circulation. The present study uses precipitation and LH estimates based on moisture budgets from Johnson and Ciesielski (2002). These datasets were obtained from the Colorado State University SCSMEX data archives (online at http://tornado.atmos.colostate.edu/scsmex/). Because there was better sounding coverage and data continuity over the NESA region (i.e., 17°–22°N, 110°–120°E) from 6 May to 20 June 1998, average gridded LH data fields from this region and for this period are compared with the TRMM CSH and TMI 2A12 LH fields.

3. LH variability in the South Asian monsoon region

Figure 1 shows the vertically integrated December–February (DJF) and June–August (JJA) seasonal averages of TRMM CSH LH for the 1998–2006 period. The most noticeable characteristic is the similarity of the LH distribution and the global surface precipitation climatology. As expected, the magnitude of LH is higher where precipitation is abundant and lower in regions of scant precipitation. Regions located over the western Pacific warm pool, the South Pacific convergence zone (SPCZ), and the northeast tropical Pacific intertropical convergence zone (ITCZ) all correspond to regions with large latent heat release. During southern summer, similar values of LH are found over the tropical continental Amazon. Slightly lower heating is found over central and southern Africa. Overall, the highest integrated LH release occurs in the Asian monsoon region, outlined in Fig. 1. Within this region, the largest LH magnitudes occur over the Bay of Bengal (BoB) during JJA. Given the overall amplitude of the LH distribution in this region, this study will concentrate on the analysis of the interannual and intraseasonal variability of heating during the summer South Asian monsoon.

Figure 2 shows longitudinal sections of climatological vertical profiles of LH for the highly convective regions of the Indian monsoon (5°–22°N, 70°–100°E), Australian monsoon (17°–0°S, 120°–150°E), the SPCZ (20°–0°S, 160°–179°E), and the east Pacific ITCZ (0°–20°N, 125°–80°W) averaged over the period 1998–2006, as well as longitudinal averages for each year. Evidence of the interannual variability of LH is apparent in all four regions. It is quite evident that the lowest values of LH release over the SPCZ in 1998 correspond to the highest values in the same year over the ITCZ region and are related to the 1997/98 El Niño event. The year 2002 was western Australia's fourth driest year in a century (Australian Bureau of Meteorology; information online

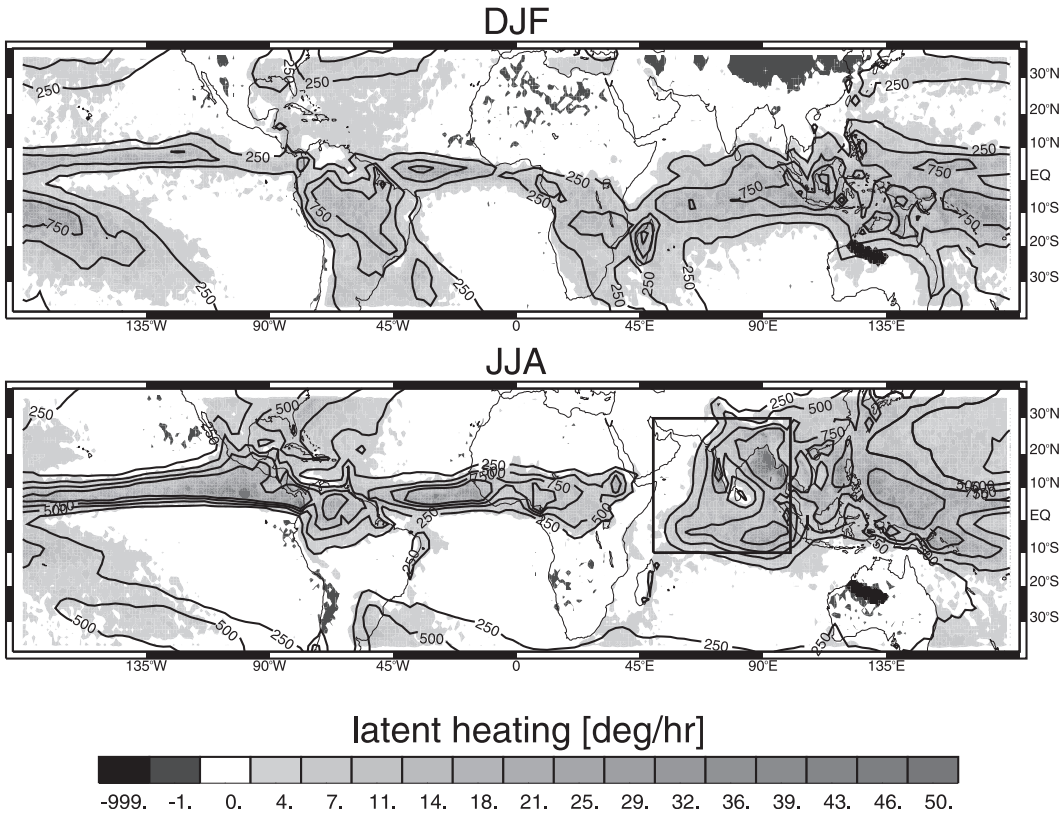

FIG. 1. Vertically integrated LH distribution (° h^{-1} relative to the shade key) for boreal (JJA) and austral (DJF) summers averaged over the 1998–2006 period using the monthly TRMM CSH dataset. Black contours show mean seasonal precipitation (mm) using monthly GPCP data. The black box corresponds to the South Asian monsoon region that is the focus of the study.

at http://www.bom.gov.au). This period of rainfall deficiency coincides with the lowest LH values (Fig. 2b, left panel). Differences in vertical profiles are also noticeable among all of the regions. While all of the profiles have a LH peak at about 7 km, the maximum value varies considerably throughout the regions. The SPCZ (Fig. 2c, left panel) and Australian monsoon (Fig. 2b, left panel) regions show the highest average values and also possess the largest interannual variability.

The annual distribution of rainfall in the SAMR exhibits a maximum peak during the summer boreal season. The JJA mean precipitation distribution (Fig. 1) shows three major zones of maximum precipitation within the monsoon trough: the northern BoB, the Western Ghats (WG), and the eastern equatorial Indian Ocean (e.g., Webster et al. 1998; Goswami and Mohan 2001). Figure 3 shows the vertically integrated LH anomaly for each year from 1998 to 2006 over the SAMR. Climatologically, maximum values of heating occur over the BoB and the central–eastern equatorial Indian Ocean (EIO) and, at a lower magnitude, over the WG. These are key areas for understanding the nature of the climatology of the entire monsoon region, especially in relation to interannual-to-intraseasonal variations (Hoyos and Webster 2007). While the climatological features are robust from year to year, high interannual variability is also evident over the entire domain with extremes values of LH in 1998, 2005, and 2006. This variability is particularly apparent over the EIO and BoB regions. The interannual and intraseasonal variability of LH in the SAMR are now described in more detail.

a. Interannual variability

Figure 4 shows the latitudinally averaged LH profiles for the 1998–2006 extended summer periods (May through September) over the BoB, EIO, WG, and central India (CI) (right panels), together with their corresponding LH average profiles (left panels). Larger LH values are observed in the BoB compared with those for the EIO, WG, and CI regions. The BoB region (Fig. 4a, left panel) has a single LH maximum at about 7 km in height. The EIO region (Fig. 4b, left panel), on the other hand, has an LH peak at the same level but with a lower-level secondary maximum. The difference between these two profiles may

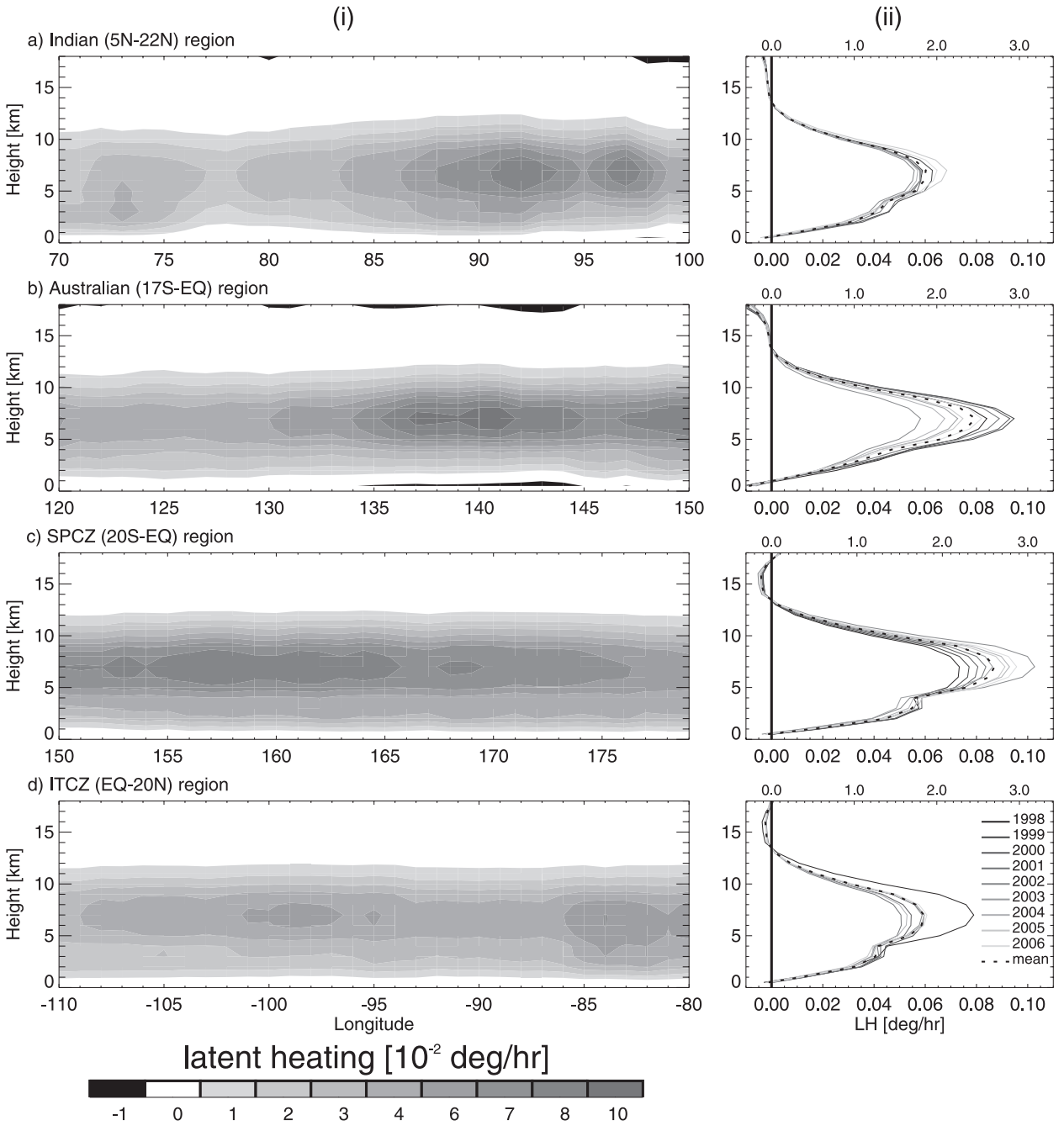

FIG. 2. (left) Longitude–height distributions and (right) the average vertical profile of LH (° h^{-1}) for each year of the 1998–2006 profiles for the (a) Indian (5°–22°N, 70°–100°E) and (b) Australian (0°–17°S, 120°–150°E) monsoon regions, (c) SPCZ (0°–20°S, 160°–179°E), and (d) east Pacific ITCZ (0°–20°N, 125°–80°W) regions using monthly TRMM CSH retrievals. Average LH profiles (dashed lines) and yearly profiles (shaded lines) are represented.

be attributed to the regional predominance of different cloud-top heights. More mature and well-developed systems (i.e., those with convective cells and well-developed stratiform precipitation aloft) are usually located over the EIO region (Haynes and Stephens 2007; Zuidema and Mapes 2008). In general, a profile shape is the combination of the two levels of heating. The lower level is associated with convective latent heat release and the higher level with stratiform LH (e.g., Fig. 3 of Schumacher et al. 2004). The combination of different levels of heating resulting from different types of precipitation will be discussed in section 4.

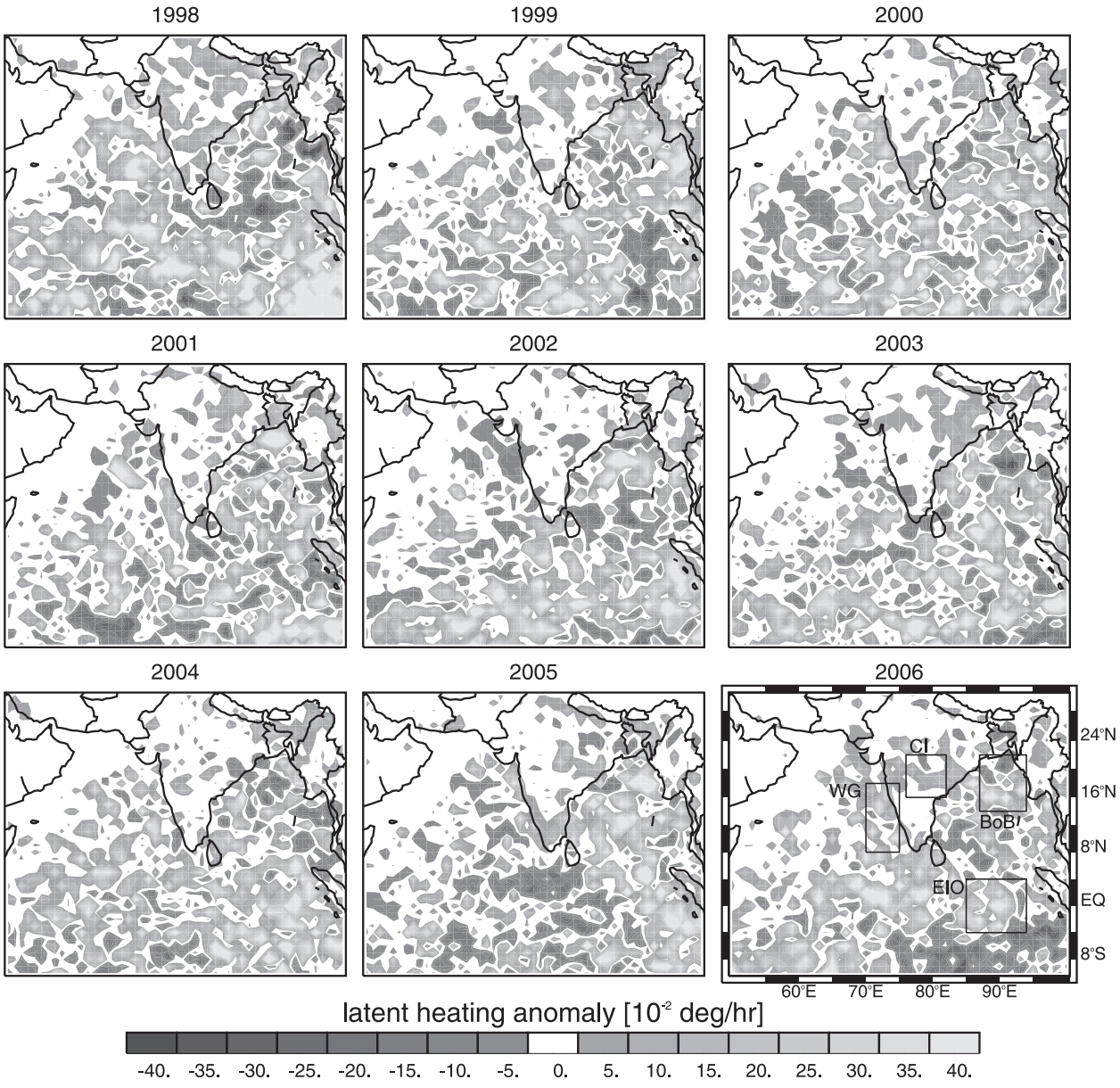

FIG. 3. Vertically integrated LH anomalies (° h^{-1}) for each year between 1998 and 2006 for the SAMR using monthly TRMM CSH data. Dark gray (light gray) corresponds to negative (positive) LH anomalies. The boxes in the lower-right corner correspond to the regions considered in this study: BoB, EIO, WG, and CI.

The averaged LH profiles for the WG region are presented in the left panel of Fig. 4c and show a distinctive difference from the other profiles. Compared to the usual maximum at 7 km (Figs. 4a,d) the maximum is at 3 km. The lower peak is related to orographically induced convection west of the WG mountain range. The configuration of mountains (mean elevation 1200 m) along the western coast of India acts as a barrier to the southwesterly monsoon flow, invoking mechanical lifting and copious precipitation (Grossman and Durran 1984; Xie et al. 2006; Hoyos and Webster 2007). A similar orographic effect is apparent in the vicinity of the elevated topography of Sumatra (the eastern part of the EIO region) located at the western edge of the Indonesian Maritime Continent (Shibagaki et al. 2006). The reason for the weak low-level heating peak is the uplift of the equatorial westerly flow by the Sumatra highlands. Similar orographically induced heavy rainfall occurs along the eastern coast of the BoB (Xie et al. 2006; Hoyos and Webster 2007). However, in contrast to the WG and EIO

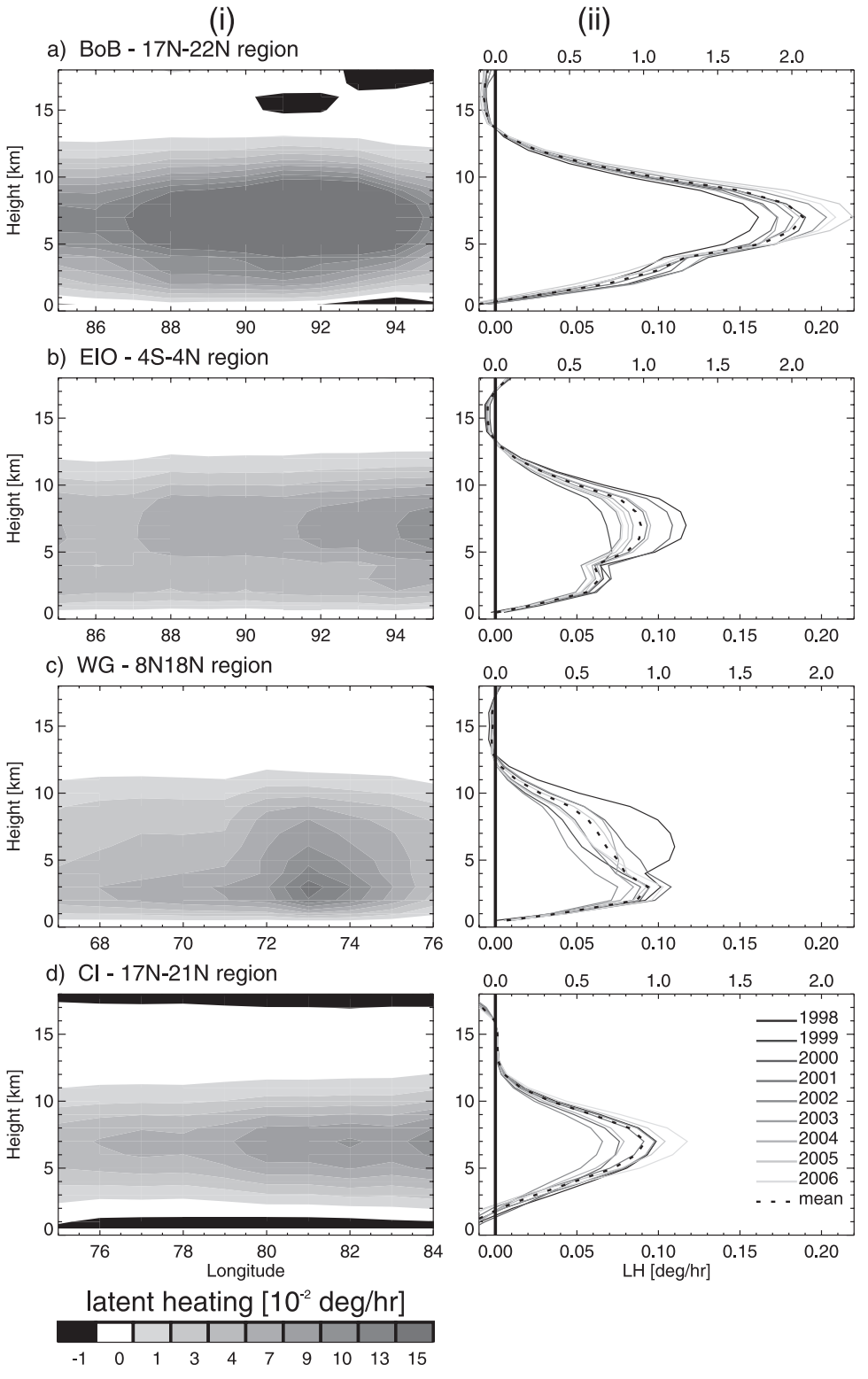

FIG. 4. Same as Fig. 2, but for extended summer periods over (a) BoB, (b) EIO, (c) WG, and (d) CI.

regions, the BoB LH profile does not show a marked lower peak. This different signature is attributed to the different type of cloud organization. Larger and deeper systems often occupy the BoB (Zuidema and Mapes 2008) spanning larger areas over the bay than systems over the Arabian Sea (Xie et al. 2006).

Figure 4 (left panels) shows that about 30% of the total 1998–2006 LH variance is explained by interannual variability. In general, monsoon precipitation variance associated with El Niño–Southern Oscillation (ENSO) was considered about 30%, with El Niño linked to a weaker monsoon and La Niña to wetter summers (Shukla and Paolino 1983). However, the monsoon–ENSO relationship appears to be nonstationary, and the translation of percent variance to actual variance yields a relatively small actual interannual variability of rainfall (~24 mm out of the mean 850-mm rainfall for India) associated with ENSO (e.g., Webster et al. 1998; Kumar et al. 1999). Moreover, predictions of interannual monsoon rainfall and river discharge using just ENSO as a predictand have limited skill (e.g., Torrence and Webster 1999; Clark et al. 2000; Jian et al. 2009). In summary, not all monsoon rainfall variability can be explained simply by the phase of ENSO, and other factors such as regional SST variability in the Indian Ocean appear to play a more important role (e.g., Harzallah and Sadourny 1997; Webster et al. 1999; Clark et al. 2000, 2003).

In addition to external factors, internal variability of the monsoon system also results in interannual anomalies of seasonal rainfall. In particular, interannual variability of the summer intraseasonal oscillation (ISO) modulates the overall summer monsoon precipitation with anomalies larger than those attributable to factors such as ENSO (Webster and Hoyos 2004; Hoyos and Webster 2007). While the limited length of the LH record does not permit a sufficiently conclusive study that would allow a separation of external and internal interannual modulation of the monsoon system, it may be possible to diagnostically link the temporal variability of the LH sample with interannual and intraseasonal modes of variability.

The magnitude of interannual variability is comparable among all of the regions examined (Fig. 4). Maxima occur during 2005 and 2006 and minima occur in 1998 and 2000 over the BoB region. The years 1998 and 2000 correspond to the maximum values of LH for the EIO. Minimum values occur in 1999 and 2002. For the WG, 1998 and 2002 are maximum and minimum years, respectively, while for the CI region, they are 2006 and 2002, respectively. Because the release of LH is directly related to precipitation, according to the canonical precipitation response to ENSO (Ropelewski and Halpert 1987; Curtis et al. 2002), one would expect that during El Niño years there would be less-than-average LH release (and the contrary for La Niña years), given the proximity of the selected regions and the large-scale nature of the ENSO–monsoon relationship. Summer (May through September) SST anomalies in the Niño-3.4 region were negative for 1998–2000 (La Niña years) and positive for 2002, 2004, and 2006 (El Niño years; online at http://www.cpc.noaa.gov). If one tries to match these years with regional maximum and minimum LH release, no coherent pattern emerges in the interannual variability associated with El Niño–La Niña years.

Studies (e.g., Goswami 1998) have suggested that a significant fraction of the interannual variability of the seasonal mean Indian summer monsoon is governed by internal dynamics through, for example, low-frequency feedbacks involving surface processes (Webster and Chou 1980; Webster 1983; Srinivasan et al. 1993). Furthermore, statistics of the monsoon intraseasonal oscillation suggest that the phenomenon influences both the seasonal mean monsoon and interannual variability (Krishnamurthy and Shukla 2000; Goswami and Mohan 2001). Hoyos and Webster (2007), using data from the Global Precipitation Climatology Project (GPCP) products (Adler et al. 2003), suggested that year-to-year changes in seasonal rainfall between different regions of the South Asian monsoon do not appear to be highly interrelated. They interpret this observation as the strong intraseasonally induced internal interannual variability of the monsoon system, concluding that rainfall anomalies associated with monsoon intraseasonal activity can be regarded as the most important internal modulator of interannual monsoon variability. The LH structures presented in Fig. 4 show that the years of maximum and minimum LH are closely associated and in better agreement with the cumulative intraseasonal oscillation rainfall patterns for the same regions (see Fig. 5 in Hoyos and Webster 2007) than with the canonical response of the monsoon to ENSO. Rainfall anomalies in the 25–80-day band were positive over the EIO (BoB) region for 1998 (2002) and 2000 (2005) and negative for 1999 (1998) and 2001 (2000). These years correspond for the most part with the years of maximum and minimum LH in these regions, reinforcing the hypothesis that externally induced interannual variability (e.g., ENSO forcing) is not the only modulator of LH variability. Intraseasonal variability emerges as an important internal modulator of the precipitation and interannual variations of LH. As such, this internal modulation, which determines the magnitude of the largest summer LH release, could affect both regional and global circulation anomalies.

b. Intraseasonal variability

Although EIO rainfall is relatively constant during the year, and as such does not possess the distinctive

seasonal cycle as found farther north in the monsoon region, it is considered to be the principal source region of monsoon intraseasonal variability (e.g., Webster et al. 1998; Lawrence and Webster 2002; Wang et al. 2005, 2006). This variability generates active and break periods over Southeast Asia on a 25–80-day time scale and is referred to as the monsoon intraseasonal oscillation (MISO), or the summer manifestation of the Madden–Julian oscillation (MJO; Zhang 2005). In general, the MISO develops first in the western equatorial Indian Ocean, propagates eastward along the equator to the eastern equatorial Indian Ocean, and then northward toward Southeast Asia and eastward along the equator to the west Pacific Ocean, modulating convective activity over the Pacific warm pool as well as over the South China Sea (e.g., Fukutomi and Yasunari 1999; Zhang 2005). There is also an equivalent southward cross-equatorial propagation from the eastern Indian Ocean, but this appears to die out quite rapidly over the cooler waters of the South Indian Ocean (Lawrence and Webster 2002; Wang et al. 2005).

1) Spatial distribution

Figure 5 shows composites of vertically integrated LH anomalies for the extended winter season of November through March (NDJFM; referred to as winter: Figs. 5a,b) and the extended summer season of May through September (MJJAS; referred to as summer: Figs. 5c,d) using the daily TRMM CSH dataset for the 1998–2006 period. Extended seasons were chosen to maximize the number of active and break events. Global merged precipitation (GPCP) data for the entire Asian monsoon region were filtered in the intraseasonal band (25–80 day) to classify the days of active and break periods. Active periods are defined as those where rainfall anomalies in the intraseasonal band are positive, on average, over the EIO region. Conversely, break periods are defined as those where rainfall anomalies are negative over the EIO region. In total, 28 (34) active periods and 24 (32) break periods are used in the winter (summer) composites. The LH anomaly composites are computed based on the days of occurrence of active and break periods over the EIO region. To emphasize the MISO-related anomalies, for each composite the mean seasonal climatology has been subtracted.

An intriguing characteristic of the summer composites is the north–south dipole of LH anomalies between the EIO and BoB regions. In general, during active periods, positive anomalies of LH appear over the EIO region in both seasons. The LH dipole has a reversed polarity during break periods. This contrasting situation during summer active and break periods suggests that intraseasonal variability strongly modulates the LH distribution over the region. During winter the propagation associated with ISO is mostly eastward and thus does not modulate convection significantly over the BoB.

2) Vertical distribution and time evolution of LH profiles

Figure 6 shows the mean summer LH profiles for the active and break monsoon periods. The out-of-phase dipole structure between the BoB and EIO is very apparent in the vertical profiles for both phases of MISO. Also, it is noteworthy that the amplitude of the intraseasonal variability (i.e., difference between the active and break profile) has a magnitude comparable to the amplitude of the interannual variability (see Fig. 4). LH MISO anomalies peak over the BoB and EIO regions near 7 km. There is a secondary peak around 3 km that is more apparent over the EIO than BoB. The main difference between the active and break vertical LH profiles is the amount of heating in each phase. During the active phase there is considerably higher heating at upper levels over the EIO region, with an incipient lower-level peak. During the break phase (Fig. 6d) the double peak is not as noticeable because of a considerable reduction in upper-level heating, while the lower-level peak remains relatively constant. The permanence of the lower-level peak suggests that orographic-induced heating acts both during the break and active phases. The overall differences suggest that over the EIO region stratiform heating aloft is considerably higher during the active phase than during the break phase. For the BoB, both phases have peaks around 7 km associated with the larger and deeper systems usually located in this region with only differences in the magnitude, suggesting that the main influence is the amount rather than the type of precipitation.

Figure 6 also shows time–height composites of LH anomalies through the active and break phases of the monsoon in the BoB and EIO regions for the 1998–2006 summer seasons. Day 0 corresponds to the date of the maximum anomalies for both the active and break phases. A most interesting feature is the development of low-level positive LH anomalies 10–15 days prior to the active (break) phase for the EIO (BoB) region at day 0 (Figs. 6c,e). Heating then diminishes until a break (active) phase is reached about 10 days after the maximum heating anomalies. Similarly, negative LH anomalies start to appear 10–15 days before the break (active) phase reaches its minimum value for the EIO (BoB) region (Figs. 6b,f). The buildup of LH anomalies represents an increase in condensational heating generated by convective activity in the early stages of precipitation. This behavior is in agreement with the observed in situ evolution of the LH observed during TOGA COARE associated with the life cycle of the MJO (Lin et al. 2004)

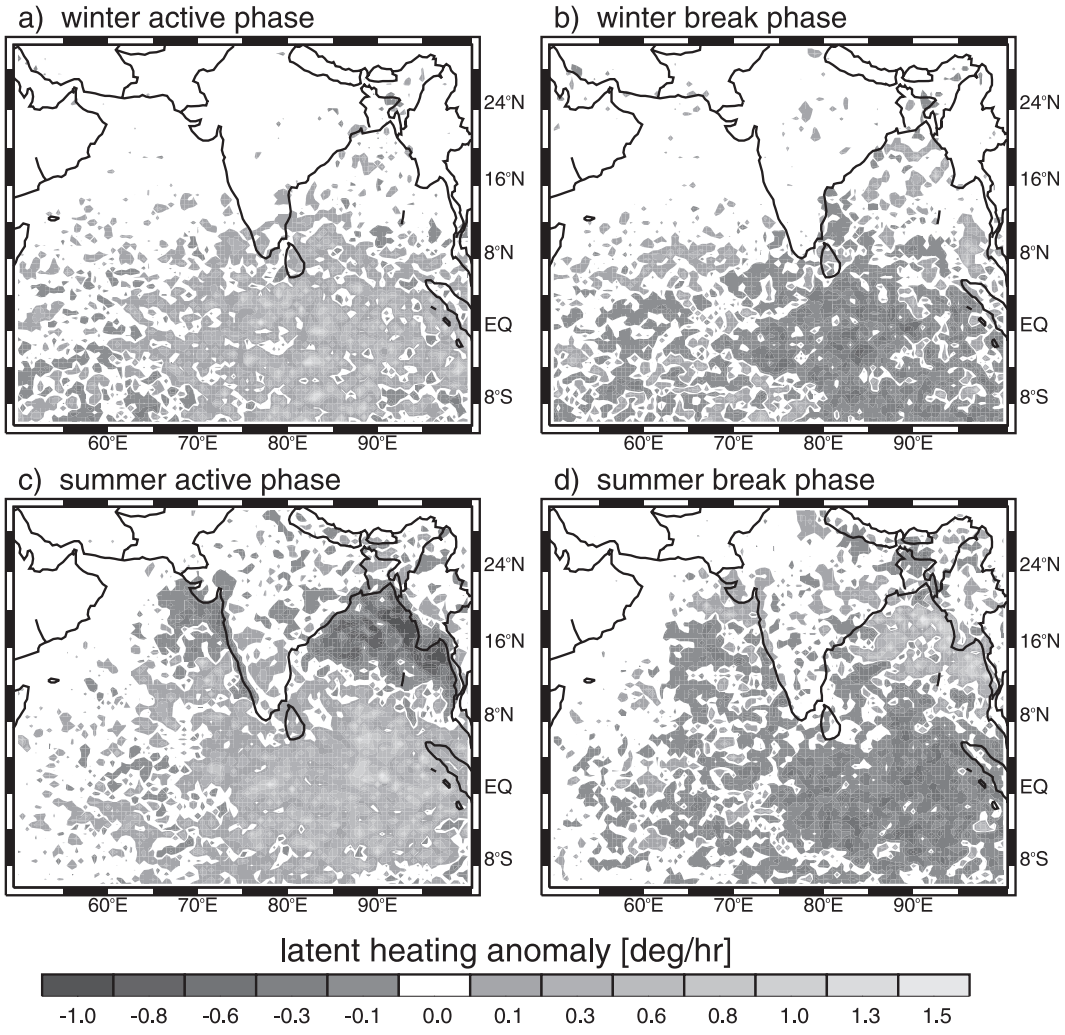

FIG. 5. Composites of vertically integrated LH anomalies (° h^{-1}) for (a),(c) active and (b),(d) break phases of the intraseasonal oscillation of the SAMR for the extended winter season (NDJFM) and extended summer season (MJJAS), respectively. Shading is relative to the scale at the bottom of the figure. The daily TRMM CSH dataset for the 1998–2006 period was used in this figure.

and is consistent with the destabilization phase of the MJO sequence of Stephens et al. (2004). In the TOGA COARE case, shallower convective heating appears in the earlier stages of the cycle with deeper convective heating occurring later in the more disturbed periods. In addition, during the latter stages, the stratiform heating becomes increasingly important and remains after the disturbed period has passed. The LH buildup occurs in association with low-level atmospheric moistening prior to the precipitation maximum and is a common feature of the transition between the suppressed (i.e., break) and active phases in intraseasonal variability during the TOGA COARE observational period (Agudelo et al. 2006).

An increase in negative LH anomalies is observed prior to day 0 for the active phase in the BoB and the break phase in the EIO (Figs. 6b,f). This is caused by a combination of two factors. The first is the presence of residual high-level stratiform precipitation from the previous disturbed period, which produces positive heating at higher elevations and cooling at lower altitudes. The second factor is the reduced surface evaporation resulting from the reduction in surface temperature by negative cloud–radiation feedback (Stephens et al. 2004; Agudelo et al. 2006).

c. Comparison with TMI 2A12 datasets

1) AVERAGE LH PROFILES

The TMI 2A12 dataset is now compared with the TRMM CSH results presented above. It is important to reemphasize that comparisons between the two datasets

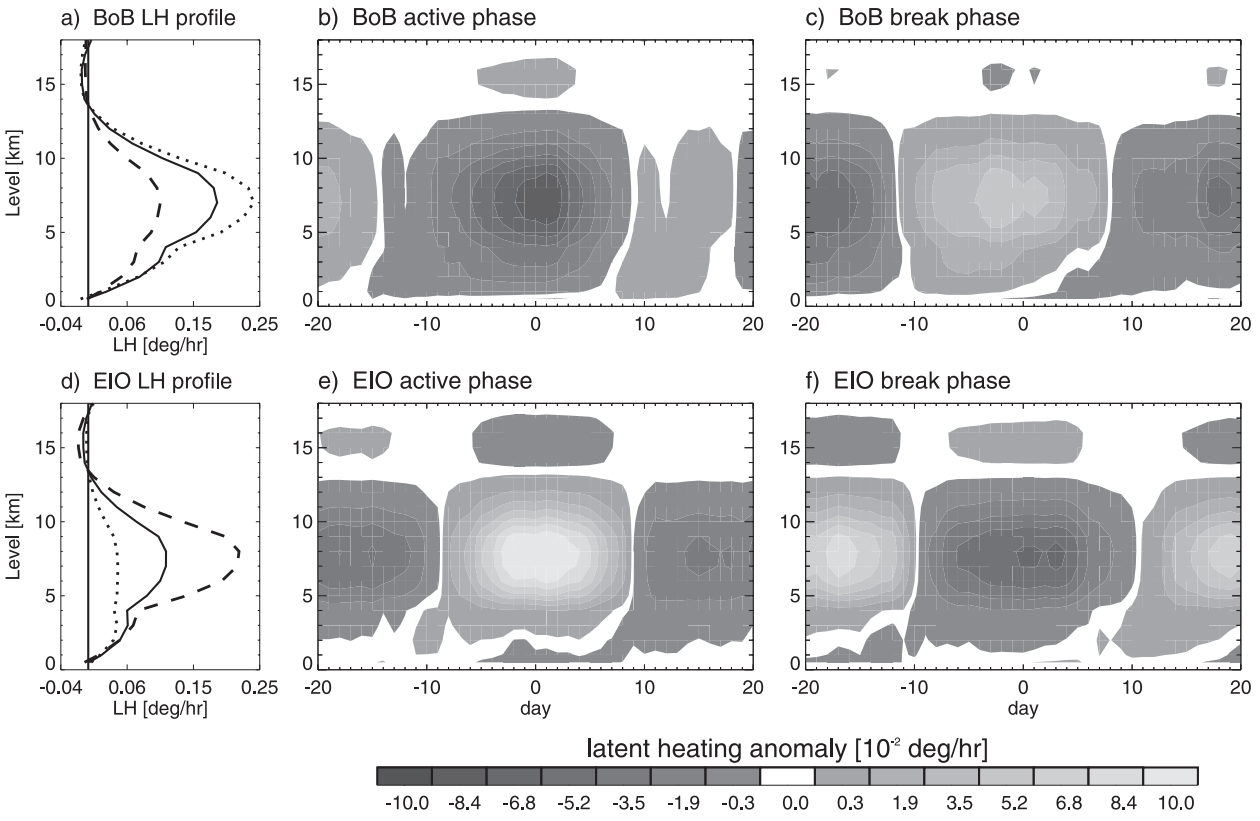

FIG. 6. (left) Mean summer LH profiles (black solid line) and mean profiles for the active (dashed line) and break periods (dotted line) of the MISO over the (a) BoB and (d) EIO regions. (right) Time evolution composites of summer LH (° h^{-1}) anomalies (time–height diagrams) ±20 days of the day 0 active/break conditions defined in the text. The TRMM CSH daily dataset for 1998–2006 summer seasons was used. The (top) BoB and (bottom) EIO regions are shown.

are limited to oceanic regions because of the unavailability of TMI 2A12 data over land. Figure 7 shows latitudinal averages and vertical profiles of LH for the BoB and EIO regions using both datasets for the extended summer periods from 1998 to 2006. The figure shows a general correspondence in the location and magnitude of the LH maximum at 7 km in height. However, there are striking differences in the shape of the vertical profile. The TMI 2A12 profiles show a narrower heating peak in a band between 6 and 9 km in height compared to the broader heating peak in the TRMM CSH profile that extends over most of the troposphere. In addition, TMI 2A12 data show cooling in the first 1 km and heating above 13 km that is not present in the TRMM CSH dataset. In contrast, the TRMM CSH profiles show positive values (i.e., heating) near the surface and zero to negative (cooling) values aloft. In addition, a pronounced heating minimum of ~5 km in height is evident in the TMI 2A12 profiles for both the BoB and EIO regions. This feature is common for most tropical areas (not shown here) and is absent in the TRMM CSH profiles. Diagnostic heating budgets based on rawinsonde, satellite, and surface data analyses have shown for the western Pacific region that the heating profiles have predominantly a single peak located between 7 and 8 km (e.g., Yanai et al. 1973; Frank et al. 1996; Lin and Johnson 1996). The two-peak shape in TMI 2A12 was evident in previous LH estimates based on the GPROF algorithm (Tao et al. 2001; Yang et al. 2006; Morita et al. 2006; Tao et al. 2006) and has been attributed to problems in the CRM database associated with high biases in the precipitation water content produced by the CRM simulation (Yang et al. 2006). These biases lead to a tendency of the GPROF algorithm to select heating profiles corresponding to a particular tropical squall line in the GCE simulations, which exhibits a relative minimum in heating in the midtroposphere, thus producing two peaks in heating (Tao et al. 2001). Variations in the height of the heating peak have significant implications for large-scale circulations in the atmosphere (e.g., Houze 1982; Hartmann et al. 1984). Model circulation anomalies assessed using different levels of heating show different responses in terms of the elevation of the circulation centers (e.g., Schumacher et al. 2004). Thus, correct assessments of the vertical distribution

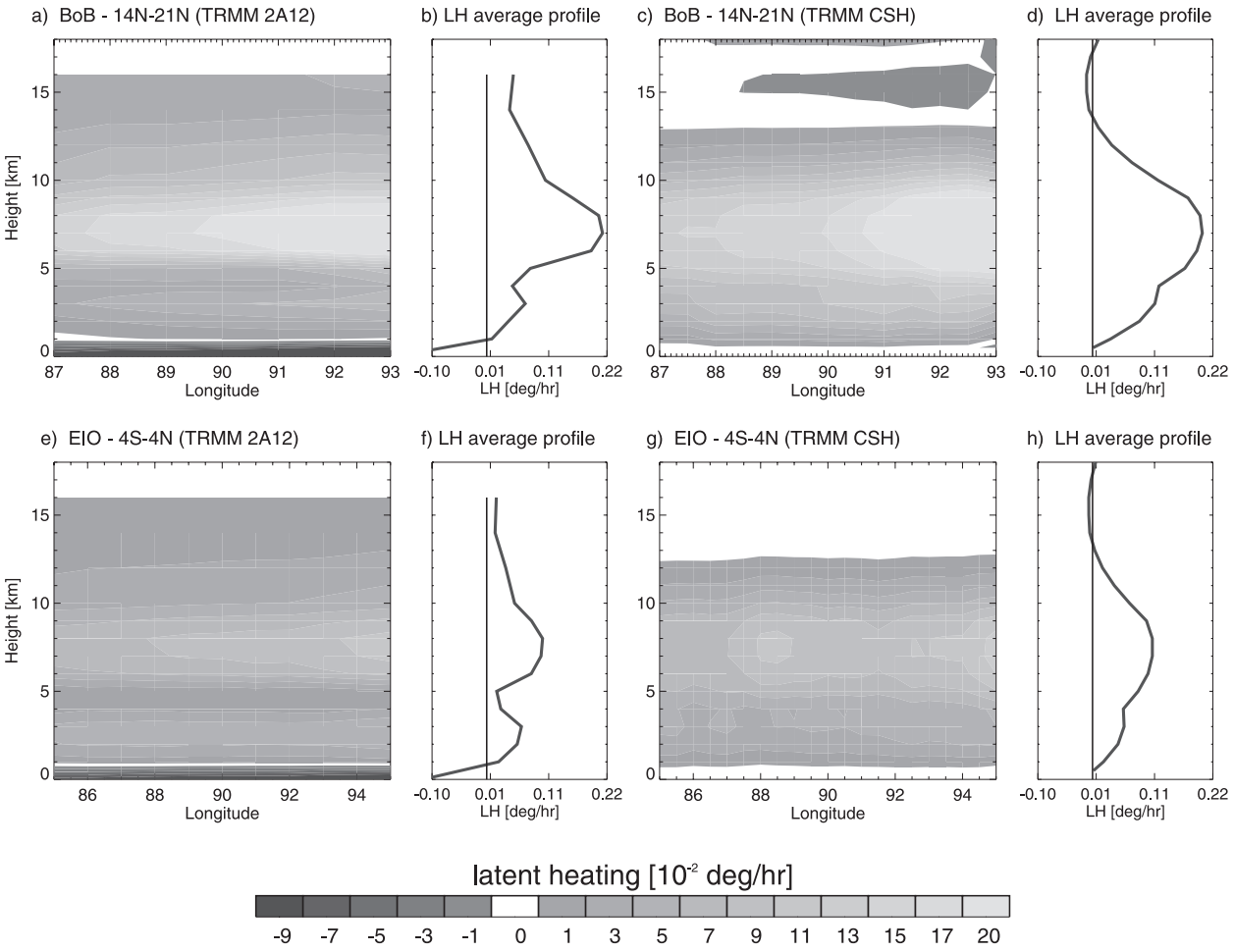

FIG. 7. Vertical distribution of latitudinally averaged LH (° h^{-1}) for the (top) BoB and (bottom) EIO regions using both the (left) TMI 2A12 and (right) TRMM CSH datasets. Extended summer periods for the 1998–2006 period for both datasets were used. The mean LH vertical profile is shown next to each panel.

of heating will lead to better simulations of the large-scale circulation structures. To verify the vertical distribution of LH in the monsoon region further, specific comparisons are made with observational field experiment measurements.

2) INTRASEASONAL VARIABILITY

Figure 8 shows composites of summer TMI 2A12 LH anomalies for active and break periods for the period 1998–2006. A comparison with Figs. 5c,d indicates a similar intraseasonal signal with a high level of correspondence between the two datasets. Both datasets produce a dipole between the BoB and EIO regions, indicating that the TMI 2A12 dataset also captures the intraseasonal signal present over the SAMR. The main difference is that the TRMM CSH variability has higher amplitude than the TMI 2A12 constructions.

3) VERTICAL DISTRIBUTION AND TIME EVOLUTION OF LH PROFILES

Figures 9a,d show the mean summer TMI 2A12 LH profiles as well as the average active and break profiles. An out-of-phase dipole structure, similar to that found in Fig. 6, is also found here, with stronger and weaker heating during the active phase over the EIO and BoB regions, respectively. All of the profiles obtained from TMI 2A12 have the same heating minimum around 5 km, as discussed earlier. However, there is a general correspondence in the magnitude of heating between these profiles and those obtained using the TRMM CSH dataset shown in Figs. 6a,d.

Figures 9b,c,e,f show the BoB and EIO time–height composites of the evolving TMI 2A12 LH anomalies constructed similarly to those shown in Fig. 6 for the TRMM CSH. Negative and positive anomalies also

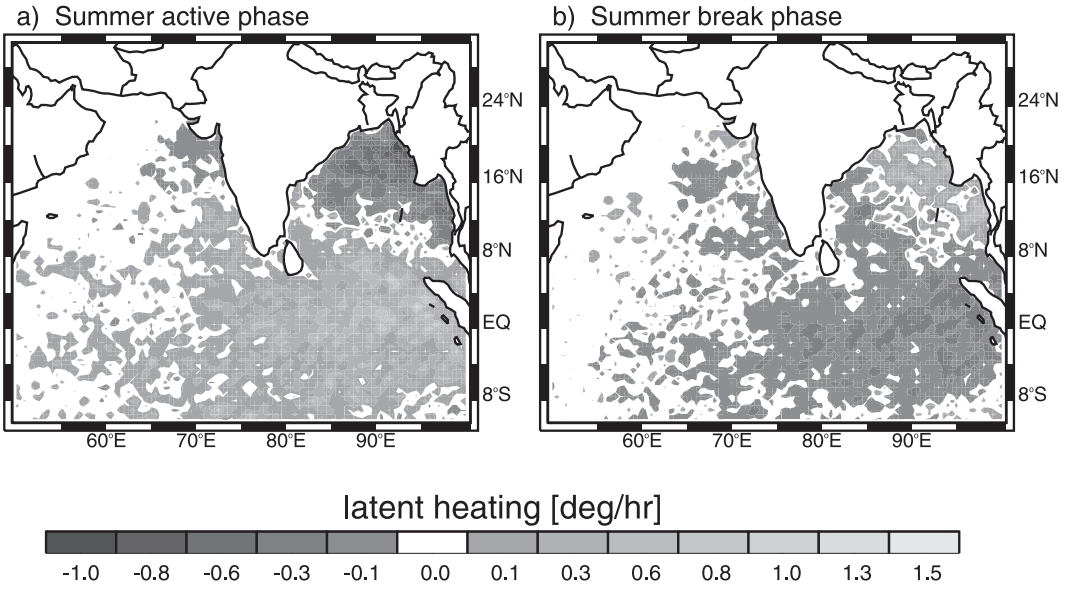

FIG. 8. Same as Fig. 5, but using the TMI 2A12 dataset.

develop about 10 days before day 0 in each region. The same progression of LH anomalies in an active–break–active cycle is evident in all of the patterns. In addition, composites for the BoB region during the break phase (Fig. 9c) and the EIO region during the active phase (Fig. 9d) also show the gradual buildup of positive convective heating anomalies. Both datasets are able to represent the increase in condensational heating at

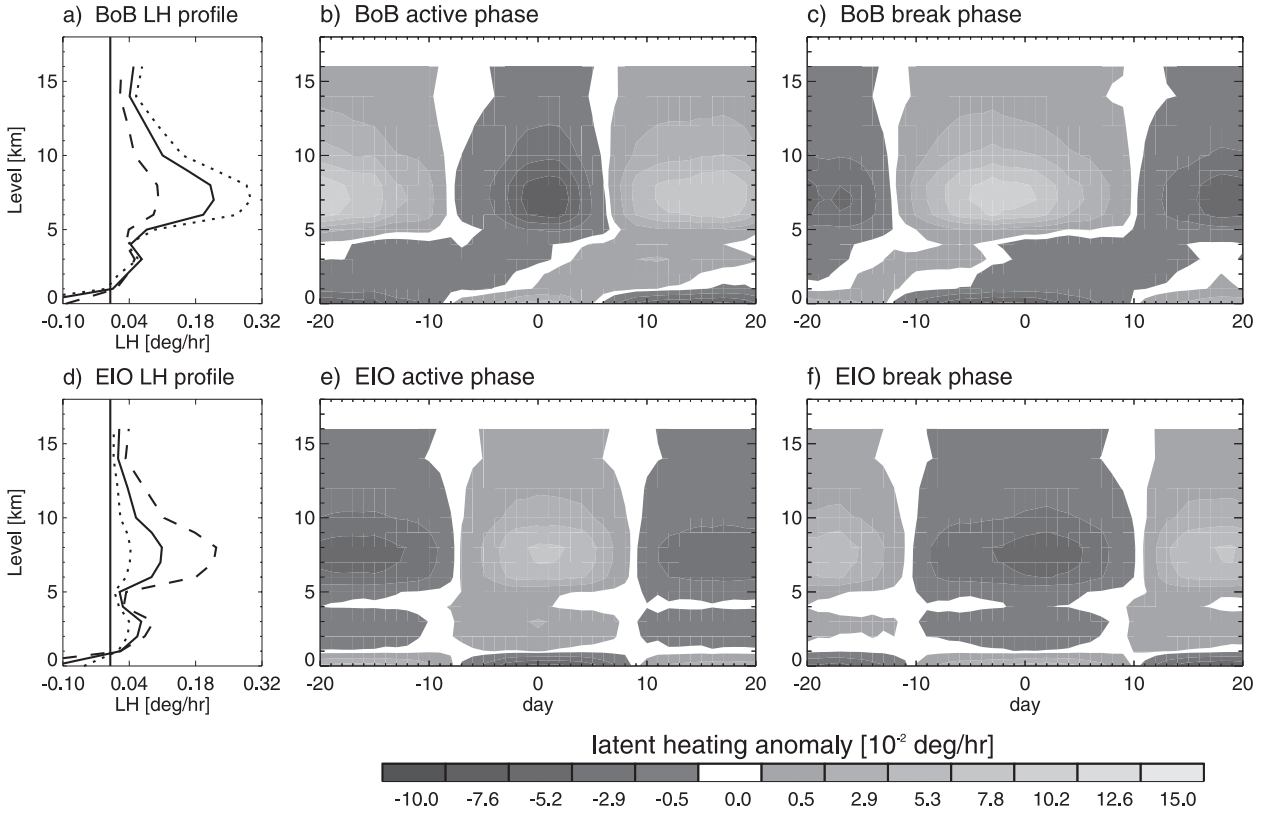

FIG. 9. Same as Fig. 6, but using the TMI 2A12 dataset.

lower levels in response to the moistening of the atmosphere prior to the development of deep convection as well as the occurrence of the disturbed period in terms of maximum LH. However, the unrealistic two-level peak in TMI 2A12 may limit the use of this dataset.

4. South China Sea Monsoon Experiment: Validation of TRMM CSH and TMI 2A12 retrievals

Evaluation of the TRMM CSH and TMI 2A12 LH datasets is a difficult task because of the scarcity of alternative LH datasets. The data obtained during SCSMEX constitute an important source of information for the validation, and possibly the improvement, of the physical assumptions used in the TRMM satellite retrievals. Data collected for two boreal summer months in 1998 have been used to investigate the large-scale circulation, convection, cloud structures, water cycle, and heating budgets associated with the onset of the southeast Asian monsoon (Lau et al. 2002; Johnson and Ciesielski 2002; Schumacher et al. 2007). Several studies have pointed out a well-established connection between the South China Sea (SCS) region with the circulation and convection in the entire Asian monsoon region (Yasunari 1979; Webster et al. 1998; Fukutomi and Yasunari 1999; Annamalai and Slingo 2001; Hoyos and Webster 2007). In addition, the seasonal march of the SCS monsoon has been well documented by LH and rainfall products from TRMM (Li et al. 2009).

Figure 10a shows the evolution of vertical LH profiles during the SCSMEX campaign from 5 May to 22 June 1998 using a moisture budget analysis from Johnson and Ciesielski (2002). The time series of precipitation is shown as a solid black line. Two periods of deep convection are evident, one in mid-May and the other in early June. Also, undisturbed periods occur before 14 May and after 11 June and have been attributed to intraseasonal variability over the region. Ding and Liu (2001) using OLR, precipitation, and wind fields found an excellent correspondence between the dates for the active and break periods in terms of rainfall and wind with the timing of these disturbed and suppressed periods. This indicates that the ISO is the main modulator of the variability of convection and precipitation in the SCS. With this in mind, four periods were selected for the comparison between the SCSMEX LH observations and the satellite retrievals (see periods 1–4 in Fig. 10).

Figures 10b,c show the corresponding estimates of LH using the TRMM CSH and TMI 2A12 datasets, respectively, for the same region and period used to compile Fig. 10a. There is good temporal correspondence between the episodes of positive LH that occurred in periods 2 and 3 among all of the datasets. These periods correspond to active phases of convection accompanied by high precipitation. Satellite precipitation retrieval from the 3G68 TRMM PR product is also shown in Fig. 10b. Periods with rainfall in the satellite retrievals correspond to periods with valid LH retrievals in both datasets. In contrast, the observational cooling in period 1 and the stratiform heating/cooling in period 4 are not captured by the TRMM LH datasets. During period 1, corresponding to a dry phase as is evident in both satellite and in situ rainfall measurements, the observed cooling is not captured by the CSH product because this is purely radiational, and by algorithm design the CSH does not estimate radiational heating/cooling in nonrain areas. In this case a radiation product is needed to fill this gap in the retrieval of total heating. During period 4, the budget captures latent heating by stratiform rainfall aloft that is not captured by the satellite products. The satellite products indicate zero latent heating in this period resulting from the lack of rainfall in the satellite retrievals and is thus a sampling issue. Figure 10 also shows the mean LH profiles for active periods 2 and 3. For these two periods the CSH profiles (Fig. 10e) represent the observed heating profiles quite well (Fig. 10d) in terms of both magnitude and location of the LH peak ($\sim$7 km height). The only significant difference is cooling aloft in period 2 that is not present in the CSH profiles and for which the LH retrievals indicate near-zero values above 13 km. However, this cooling does not appear to be associated with evaporation and seems to be more related with remaining clear-sky radiative cooling from the previous period, as will be explained later.

The correspondence between the observed SCMEX LH profiles and the TMI 2A12 estimates (Figs. 10d,f) is not as good as with the CSH dataset, and significant differences in the magnitude and shape of the LH profiles exist. For example, while both the observations and CSH estimates agree on the relative magnitude of the heating in each period, the TMI 2A12 data indicate a contrary situation with greater heating in period 2 than in period 3. This could be a result of the different precipitation sensor swaths used for the two retrievals. While TRMM CSH is based on TRMM PR retrievals, TMI 2A12 is based on TMI retrievals (Tao et al. 2006). Both precipitation sensors have different scanning geometries, which could influence the rain estimates and hence the average LH retrievals. In addition, TMI 2A12 estimates indicate the existence of a lower-level minimum in LH around 4 km that is not apparent in the observed LH profiles in Fig. 10d. This minimum is related to the artifact in the 2A12 algorithm regarding the selection of the LH profiles as discussed previously. In addition to the problems with the lower-level minimum,

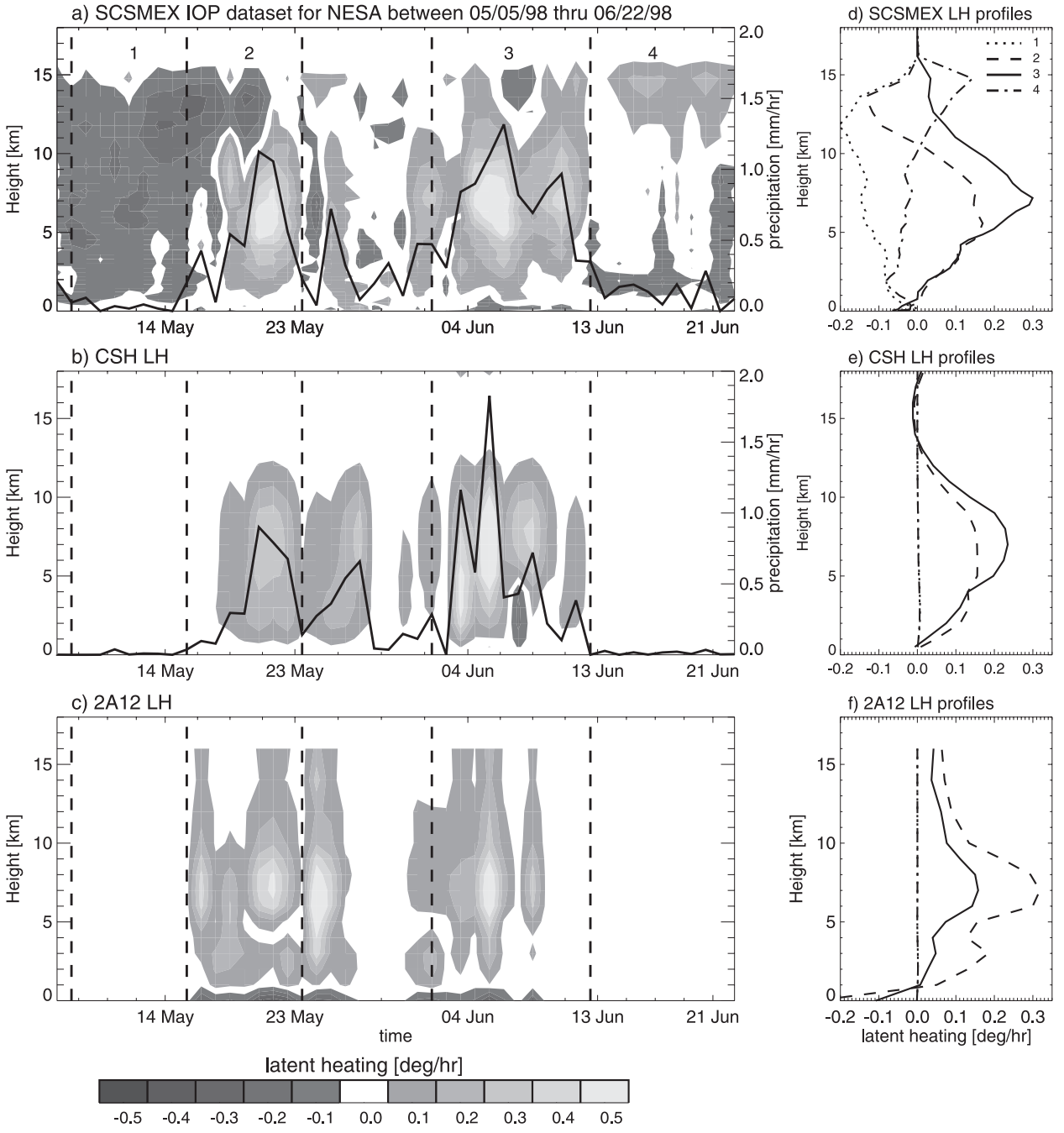

FIG. 10. Evolution of LH vertical profiles (° h^{-1}) from (a) the SCSMEX campaign from Johnson and Ciesielski (2002), (b) the TRMM CSH, and (c) the TMI 2A12 datasets during 5 May to 22 Jun 1998 over the SCS region. Light gray is proportional to positive LH values. The black line in (a) corresponds to the time series of precipitation from the SCSMEX observational period and in (b) from the TRMM 3G68 PR–based product. (right) Averaged LH profiles for four periods denoted by the vertical dashed lines in Fig. 10a using each dataset as described in the text. The periods are 7–14 May 1998, 15–23 May 1998, 1 Jun–12 May 1998, and 1 Jun–12 May 1998.

TMI 2A12 estimates show positive heating above 13 km where the observations and TRMM CSH retrievals indicate either negative or zero heating.

For the undisturbed periods, the profiles in Fig. 10d correspond to clear-sky radiative cooling (period 1) and stratiform precipitation (period 4), respectively. However, the values for period 1 represent extreme cooling with values exceeding typical clear-sky radiative values. This may be caused by subsidence induced by terrain-blocking effects across the study region despite the adjustments in

low-level winds in the moisture budget made by Johnson and Ciesielski (2002). Schumacher et al. (2007), using the same sounding information but with a different heat budget methodology, found almost the same profile shapes but greater magnitudes during the active periods than Johnson and Ciesielski (2002), and a better correspondence to profiles of clear-sky radiative cooling for the break periods. The TRMM CSH and TMI 2A12 profiles for periods 1 and 4 (Figs. 10e,f) show zero heating throughout the vertical. This is because TRMM datasets do not provide LH estimations for periods with no surface precipitation, like cases where heating is mainly produced by clear-sky radiative processes, or in the presence of nonsurface-precipitating anvils or young convection. In the first case, a radiative heating product would be necessary in order to better characterize the total atmospheric heating.

Given the considerable differences between the TMI 2A12 retrievals and observations, further validation analysis focuses on TRMM CSH estimates. The TRMM CSH LH retrieval uses a predefined LUT to calculate the vertical profiles of LH based on surface rainfall and precipitation type. Starting with precipitation type (i.e., convective or stratiform) and surface rainfall, predefined heating profiles that are normalized by surface rain rate are combined to produce the retrieved LH profiles. Figure 11a shows the rainfall-normalized LH profiles that are used to calculate LH in the TRMM CSH algorithm (i.e., lookup tables) for different type of precipitating systems (S. Lang 2000, personal communication). Only the profiles over the ocean are shown because comparisons with SCSMEX estimations are over ocean surfaces. By algorithm design, all LH estimates over the ocean in the daily and monthly CSH datasets are a linear combination of those normalized profiles.

In order for the CSH algorithm to provide accurate estimates of LH, linear combinations of the normalized profiles should be able to represent most of the observed heating profiles. Note that all of the coefficients in the linear combination are positive by algorithm design because they are associated with ratios of precipitation type (i.e., convective and stratiform fractions) relative to the total precipitation. To study the performance of the TRMM CSH retrievals relative to its design, linear combinations of the normalized profiles are used to try to represent the observed LH during the disturbed periods of the SCSMEX campaign. Figure 11c presents the observed LH profiles for four different times during the period of 15 May 15–6 June corresponding to rainy periods (21 May 2008, 25 May 2008, 1 June 2008, and 6 June 2008). These profiles were chosen to be representative of different atmospheric conditions to test whether combinations of the TRMM CSH LUT are able to reproduce the observed LH profiles. A least squares multilinear regression was used to find the coefficients of the linear combination of normalized LH profiles that minimize the root-mean-square error. In this case, the dependent variable is the observed profile and the independent variables are the normalized profiles. The adjusted profiles and the correlation coefficients for each case are also shown in Fig. 11c. The first and fourth cases correspond to the largest values of precipitation and LH and show the highest correlation values. Fitted profiles for all cases match well with the observed heating profile. All of them are a combination of profiles in the LUT with the highest correlation with the base convective heating profile (CO). For the first case, the second largest correlation is associated with the shallow convective profile (SC) while for the fourth case is associated with the stratiform profile (SO). These results from the least squares method that are used in selecting the base profiles are both statistically and physically correct. This agreement between the observations and fitted profiles using the LUT profiles for cases with positive LH confirms the utility and physical robustness of the TRMM CSH satellite-derived LH.

5. Summary and conclusions

Two satellite-derived datasets (TRMM CSH and TMI 2A12) are used to analyze the horizontal, vertical, and temporal distribution of LH over tropical regions and, in particular, over the South Asian monsoon region. The emphasis of the study is on the interannual and intraseasonal variability in the LH signatures. In terms of general LH distribution, the CSH dataset corresponds quite well with the mean tropical rainfall distribution. The Asian monsoon region, especially in the Bay of Bengal, shows the most striking seasonal contrast, with LH going from zero values during DJF to a global maximum during JJA.

No coherent large-scale interannual pattern of LH variability was found in subregions of the Asian monsoon region. In other words, global-scale teleconnections, especially those associated with ENSO, do not explain the majority of the monsoonal interannual LH anomalies. The regional interannual dissimilarities appear to be the result of internal monsoon variability. Comparatively, the years of maximum and minimum LH release identified in this study correspond closely with the cumulative intraseasonal rainfall anomalies presented by Hoyos and Webster (2007). The amplitudes associated with the mean intraseasonal heating ($0.1^\circ\ h^{-1}$ on average) are comparable with the amplitudes of interannual variability. These results reinforce the hypothesis, originally posed by Ferranti et al. (1997), that distribution of rainfall anomalies

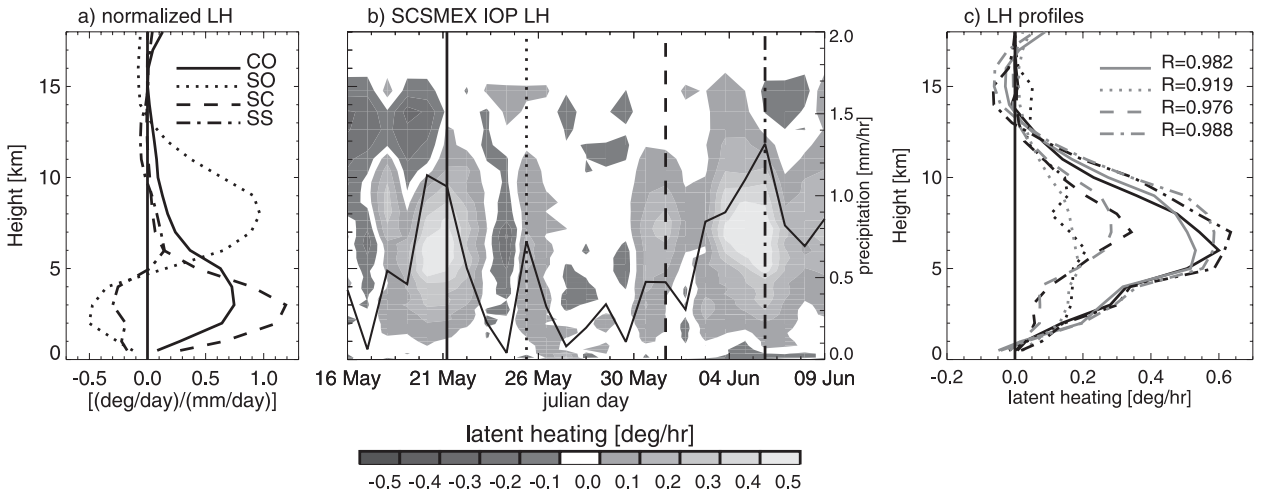

FIG. 11. (a) LH profiles basis for the CSH algorithm (i.e., LUT) for ocean convective (CO), ocean stratiform (SO), shallow convective (SC), and shallow stratiform (SS) precipitating systems. Profiles are normalized by rainfall rate ($^\circ$ day^{-1}) (mm day^{-1})$^{-1}$. (b) Evolution of LH vertical profiles ($^\circ$ h^{-1}) from the SCSMEX NESA dataset from 16 May to 9 Jun 1998 over the SCS region. Light gray is proportional to positive LH values. (c) LH profiles estimated for the 4 days (21 May 2008, 25 May 2008, 1 Jun 2008, and 6 Jun 2008) represented by vertical lines in (b) using the SCSMEX dataset (black line) and computed using multilinear regression (gray lines) from the normalized profiles in (a).

associated with monsoon intraseasonal activity are the most important internal mode of variability that modulates interannual monsoon variability.

Because of the importance of the intraseasonal variability in the region, temporal composites were constructed to analyze the LH–ISO relationship. It is concluded that the LH satellite-derived datasets exhibit clear canonical signals of the life cycle of intraseasonal oscillations. Composites of LH anomalies show a clear north–south LH dipole between the EIO and BoB regions during active and break phases of the ISO. The time–height composites of LH intraseasonal anomalies show an upward propagation of positive convective heating anomalies during transition periods from break to active phases ~10 days prior to the maximum convection. This upward propagation is the result of the net positive buoyancy in lower levels and is a precursor to deep convection in the development of precipitation systems.

A comparison of the two TRMM datasets (TMI 2A12 and TRMM CSH) shows that both datasets provide similar results in terms of magnitude and level of maximum heating. However, the two sets differ significantly in the shape of the vertical LH profiles. For example, an anomalous LH minimum near 4 km in height appears in the TMI 2A12 retrievals. Diagnostic studies (e.g., Yanai et al. 1973; Frank et al. 1996; Lin and Johnson 1996) have shown heating profiles in this region with a characteristic single LH peak located around 7–8 km in height. This anomalous minimum appears to be an artifact of the algorithm selecting heating profiles from a particular tropical squall line from the GCE simulations within the associated LUT (Tao et al. 2001). Relative to intraseasonal variability, both datasets describe similar behavior with analogous locations of above- and below-average LH. Similar characteristics are shown for the time–height evolution anomalies of LH. However, the TMI 2A12 composites still possess a midlevel anomalous minimum, as discussed previously.

Data from the SCSMEX observational period are used to validate the vertical profiles of LH provided by the TRMM satellite retrievals. Both the TRMM CSH and TMI 2A12 latent heating retrievals show good correspondence in periods of positive LH occurrence with the SCSMEX budgets. However, dry periods corresponding to clear-sky or nonsurface-precipitating clouds are not properly represented by the LH satellite datasets because the LH algorithms are not designed to do so. The shortcoming in clear-sky cases could be overcome with the addition of another type of heating product, like the total column–integrated radiative heating proposed by L'Ecuyer and Stephens (2003), which represents the net change in column-integrated radiative heating induced by the presence of clouds and precipitation. The addition of this type of information is particularly important for a better representation of the total diabatic heating in the atmospheric column. In cases of zero LH retrieval in the existence of nonsurface-precipitating clouds, LH algorithms should consider three-dimensional precipitation retrievals in order to fully account for the total atmospheric LH.

The vertical distribution of heating in the atmosphere is an important factor driving and modulating tropical

and extratropical weather. Also, dynamical model experiments have proven that the atmospheric response is strongly dependant on the vertical profile of heating. For these reasons, an adequate description of the vertical profile of LH is an important goal in order to improve model characterizations of current and future climate dynamics. The analyses presented here show that LH algorithms based on satellite information are capable of representing the spatial and temporal characteristics of the vertically integrated heating in the Asian monsoon region. However, the vertical distribution of atmospheric heating still needs to be improved. TRMM CSH has proven to be an adequate representative of the vertical distribution. TMI 2A12 has higher biases in retrieving the correct shape of LH heating profile than TRMM CSH. A more comprehensive set of high-resolution cloud-resolving model simulations similar to those of Tao et al. (2001), but for different precipitation systems, will help improve these deficiencies.

Acknowledgments. This research has been supported from the National Science Foundation's Atmospheric Science division under NSF Grant ATM-0531771 (PJW) and by the National Oceanic and Atmospheric Administration Climate Program Office under ACC Grant GC08-027 (CDH). We thank Drs. W. K. Tao and S. Lang for providing the TRMM CSH datasets and Dr. W. S. Olson for providing the TMI 2A12 dataset. Also, we thank Profs. R. A. Houze and C. Schumacher and the anonymous reviewer B for many helpful suggestions. Some of the TRMM datasets utilized in this study were accessed from the TRMM Science Data and Information System and the Goddard Space Flight Center Distributed Active Archive Center.

REFERENCES

Adler, R. F., and Coauthors, 2003: The Version-2 Global Precipitation Climatology Project (GPCP) Monthly Precipitation Analysis (1979–present). *J. Hydrometeor.,* **4,** 1147–1167.

Agudelo, P. A., J. A. Curry, C. D. Hoyos, and P. J. Webster, 2006: Transition between suppressed and active phases of intraseasonal oscillations in the Indo-Pacific warm pool. *J. Climate,* **19,** 5519–5530.

Annamalai, H., and J. M. Slingo, 2001: Active/break cycles: Diagnosis of the intraseasonal variability of the Asian summer monsoon. *Climate Dyn.,* **18** (1–2), 85–102.

Chiang, J. C. H., S. E. Zebiak, and M. A. Cane, 2001: Relative roles of elevated heating and surface temperature gradients in driving anomalous surface winds over tropical oceans. *J. Atmos. Sci.,* **58,** 1371–1394.

Clark, C. O., J. E. Cole, and P. J. Webster, 2000: Indian Ocean SST and Indian summer rainfall: Predictive relationships and their decadal variability. *J. Climate,* **13,** 2503–2519.

——, P. J. Webster, and J. E. Cole, 2003: Interdecadal variability of the relationship between the Indian Ocean zonal mode and East African coastal rainfall anomalies. *J. Climate,* **16,** 548–554.

Curtis, S., G. J. Huffman, and R. F. Adler, 2002: Precipitation anomalies in the tropical Indian Ocean and their relation to the initiation of El Niño. *Geophys. Res. Lett.,* **29,** 1441, doi:10.1029/2001GL013399.

DeMaria, M., 1985: Linear response of a stratified tropical atmosphere to convective forcing. *J. Atmos. Sci.,* **42,** 1944–1959.

Ding, Y. H., and Y. J. Liu, 2001: Onset and the evolution of the summer monsoon over the South China Sea during SCSMEX Field Experiment in 1998. *J. Meteor. Soc. Japan,* **79,** 255–276.

Emanuel, K. A., J. D. Neelin, and C. S. Bretherton, 1994: On large-scale circulations in convecting atmospheres. *Quart. J. Roy. Meteor. Soc.,* **120,** 1111–1143.

Ferranti, L., J. M. Slingo, and T. N. Palmer, 1997: Relations between interannual and intraseasonal monsoon variability as diagnosed from AMIP integrations. *Quart. J. Roy. Meteor. Soc.,* **123,** 1323–1357.

Frank, W. M., H. J. Wang, and J. L. McBride, 1996: Rawinsonde budget analyses during the TOGA COARE IOP. *J. Atmos. Sci.,* **53,** 1761–1780.

Fukutomi, Y., and T. Yasunari, 1999: 10-25 day intraseasonal variations of convection and circulation over East Asia and western North Pacific during early summer. *J. Meteor. Soc. Japan,* **77,** 753–769.

Gill, A. E., 1980: Some simple solutions for heat-induced tropical circulation. *Quart. J. Roy. Meteor. Soc.,* **106,** 447–462.

Goswami, B. N., 1998: Interannual variations of Indian summer monsoon in a GCM: External conditions versus internal feedbacks. *J. Climate,* **11,** 501–522.

——, and R. S. A. Mohan, 2001: Intraseasonal oscillations and interannual variability of the Indian summer monsoon. *J. Climate,* **14,** 1180–1198.

Grossman, R. L., and D. R. Durran, 1984: Interaction of low-level flow with the western Ghat Mountains and offshore convection in the summer monsoon. *Mon. Wea. Rev.,* **112,** 652–672.

Hartmann, D. L., H. H. Hendon, and R. A. Houze, 1984: Some implications of the mesoscale circulations in tropical cloud clusters for large-scale dynamics and climate. *J. Atmos. Sci.,* **41,** 113–121.

Harzallah, A., and R. Sadourny, 1997: Observed lead-lag relationships between Indian summer monsoon and some meteorological variables. *Climate Dyn.,* **13,** 635–648.

Haynes, J. M., and G. L. Stephens, 2007: Tropical oceanic cloudiness and the incidence of precipitation: Early results from CloudSat. *Geophys. Res. Lett.,* **34,** L09811, doi:10.1029/2007GL029335.

Houze, R. A., 1982: Cloud clusters and large-scale vertical motions in the tropics. *J. Meteor. Soc. Japan,* **60,** 396–410.

Hoyos, C. D., and P. J. Webster, 2007: The role of intraseasonal variability in the nature of Asian monsoon precipitation. *J. Climate,* **20,** 4402–4424.

Jian, J., P. J. Webster, and C. D. Hoyos, 2009: Large-scale controls on Ganges and Brahmaputra River discharge on intraseasonal and seasonal time-scales. *Quart. J. Roy. Meteor. Soc.,* **135,** 353–370.

Johnson, R. H., and P. E. Ciesielski, 2002: Characteristics of the 1998 summer monsoon oset over the northern South China Sea. *J. Meteor. Soc. Japan,* **80,** 561–578.

Krishnamurthy, V., and J. Shukla, 2000: Intraseasonal and interannual variability of rainfall over India. *J. Climate,* **13,** 4366–4377.

Krishnamurti, T. N., and H. N. Bhalme, 1976: Oscillations of a monsoon system. Part 1: Observational aspects. *J. Atmos. Sci.,* **33,** 1937–1954.

Kumar, K. K., B. Rajagopalan, and M. A. Cane, 1999: On the weakening relationship between the Indian monsoon and ENSO. *Science,* **284,** 2156–2159.

Kummerow, C., W. Barnes, T. Kozu, J. Shiue, and J. Simpson, 1998: The Tropical Rainfall Measuring Mission (TRMM) sensor package. *J. Atmos. Oceanic Technol.,* **15,** 809–817.

Lau, K. M., and L. Peng, 1987: Origin of low-frequency (intraseasonal) oscillations in the tropical atmosphere. Part I: Basic theory. *J. Atmos. Sci.,* **44,** 950–972.

——, and Coauthors, 2000: A report of the field operations and early results of the South China Sea Monsoon Experiment (SCSMEX). *Bull. Amer. Meteor. Soc.,* **81,** 1261–1270.

——, X. Li, and H. T. Wu, 2002: Evolution of the large scale circulation, cloud structure and regional water cycle associated with the South China Sea monsoon during May–June, 1998. *J. Meteor. Soc. Japan,* **80,** 1129–1147.

Lawrence, D. M., and P. J. Webster, 2002: The boreal summer intraseasonal oscillation: Relationship between northward and eastward movement of convection. *J. Atmos. Sci.,* **59,** 1593–1606.

L'Ecuyer, T. S., and G. L. Stephens, 2003: The tropical oceanic energy budget from the TRMM perspective. Part I: Algorithm and uncertainties. *J. Climate,* **16,** 1967–1985.

Li, W., D. Wang, T. Lei, and H. Wang, 2009: Convective and stratiform rainfall and heating associated with the summer monsoon over the South China Sea based on TRMM data. *Theor. Appl. Climatol.,* **95,** 157–163.

Lin, J. L., B. Mapes, M. H. Zhang, and M. Newman, 2004: Stratiform precipitation, vertical heating profiles, and the Madden–Julian oscillation. *J. Atmos. Sci.,* **61,** 296–309.

Lin, X., and R. H. Johnson, 1996: Heating, moistening, and rainfall over the western Pacific warm pool during TOGA COARE. *J. Atmos. Sci.,* **53,** 3367–3383.

Malkus, J. S., 1962: Large-scale interactions. *The Sea: Ideas and Observations on Progress in the Study of the Seas,* M. N. Hill, Ed., John Wiley and Sons, 88–294.

Mapes, B. E., 1993: Gregarious tropical convection. *J. Atmos. Sci.,* **50,** 2026–2037.

Matsuno, T., 1966: Quasi-geostrophic motions in the equatorial area. *J. Meteor. Soc. Japan,* **44,** 25–43.

Morita, J., Y. N. Takayabu, S. Shige, and Y. Kodama, 2006: Analysis of rainfall characteristics of the Madden-Julian oscillation using TRMM satellite data. *Dyn. Atmos. Oceans,* **42,** 107–126.

Nakazawa, T., 1988: Tropical super clusters within intraseasonal variations over the western Pacific. *J. Meteor. Soc. Japan,* **66,** 823–839.

Nigam, S., C. Chung, and E. DeWeaver, 2000: ENSO diabatic heating in ECMWF and NCEP–NCAR reanalyses, and NCAR CCM3 simulation. *J. Climate,* **13,** 3152–3171.

Olson, W. S., C. D. Kummerow, Y. Hong, and W. K. Tao, 1999: Atmospheric latent heating distributions in the tropics derived from satellite passive microwave radiometer measurements. *J. Appl. Meteor.,* **38,** 633–664.

——, and Coauthors, 2006: Precipitation and latent heating distributions from satellite passive microwave radiometry. Part I: Improved method and uncertainties. *J. Appl. Meteor. Climatol.,* **45,** 702–720.

Riehl, H., and J. S. Malkus, 1958: On the heat balance in the equatorial trough zone. *Geophysica,* **6,** 503–538.

——, and J. Simpson, 1979: The heat balance of the equatorial trough zone, revisited. *Contrib. Atmos. Phys.,* **52,** 287–304.

Ropelewski, C. F., and M. S. Halpert, 1987: Global and regional scale precipitation patterns associated with the El Niño/Southern Oscillation. *Mon. Wea. Rev.,* **115,** 1606–1626.

Schumacher, C., R. A. Houze, and I. Kraucunas, 2004: The tropical dynamical response to latent heating estimates derived from the TRMM precipitation radar. *J. Atmos. Sci.,* **61,** 1341–1358.

——, M. H. Zhang, and P. E. Ciesielski, 2007: Heating structures of the TRMM field campaigns. *J. Atmos. Sci.,* **64,** 2593–2610.

Shibagaki, Y., and Coauthors, 2006: Multiscale aspects of convective systems associated with an intraseasonal oscillation over the Indonesian Maritime Continent. *Mon. Wea. Rev.,* **134,** 1682–1696.

Shukla, J., and D. A. Paolino, 1983: The Southern Oscillation and long range forecasting of the summer monsoon rainfall over India. *Mon. Wea. Rev.,* **111,** 1830–1837.

Sikka, D. R., and S. Gadgil, 1980: On the maximum cloud zone and the ITCZ over Indian longitudes during the southwest monsoon. *Mon. Wea. Rev.,* **108,** 1840–1853.

Srinivasan, J., S. Gadgil, and P. J. Webster, 1993: Meridional propagation of large-scale monsoon convective zones. *Meteor. Atmos. Phys.,* **52** (1–2), 15–35.

Stephens, G. L., P. J. Webster, R. H. Johnson, R. Engelen, and T. L'Ecuyer, 2004: Observational evidence for the mutual regulation of the tropical hydrological cycle and tropical sea surface temperatures. *J. Climate,* **17,** 2213–2224.

Sui, C. H., and K. M. Lau, 1989: Origin of low-frequency (intraseasonal) oscillations in the tropical atmosphere. Part II: Structure and propagation of mobile wave-CISK modes and their modification by lower boundary forcings. *J. Atmos. Sci.,* **46,** 37–56.

Tao, W. K., and J. Simpson, 1993: The Goddard cumulus ensemble model. Part I: Model description. *Terr. Atmos. Ocean Sci.,* **4,** 19–54.

——, S. Lang, J. Simpson, and R. Adler, 1993: Retrieval algorithms for estimating the vertical profiles of latent-heat release: Their applications for TRMM. *J. Meteor. Soc. Japan,* **71,** 685–700.

——, ——, ——, W. S. Olson, D. Johnson, B. Ferrier, C. Kummerow, and R. Adler, 2000: Vertical profiles of latent heat release and their retrieval for TOGA COARE convective systems using a cloud resolving model, SSM/I, and ship-borne radar data. *J. Meteor. Soc. Japan,* **78,** 333–355.

——, and Coauthors, 2001: Retrieved vertical profiles of latent heat release using TRMM rainfall products for February 1988. *J. Appl. Meteor.,* **40,** 957–982.

——, and Coauthors, 2006: Retrieval of latent heating from TRMM measurements. *Bull. Amer. Meteor. Soc.,* **87,** 1555–1572.

Torrence, C., and P. J. Webster, 1999: Interdecadal changes in the ENSO–monsoon system. *J. Climate,* **12,** 2679–2690.

Wang, B., P. J. Webster, and H. Teng, 2005: Antecedents and self-induction of active-break south Asian monsoon unraveled by satellites. *Geophys. Res. Lett.,* **32,** L04704, doi:10.1029/2004GL020996.

——, ——, K. Kikuchi, T. Yasunari, and Y. Qi, 2006: Boreal summer quasi-monthly oscillation in the global tropics. *Climate Dyn.,* **27** (7–8), 661–675.

Webster, P. J., 1972: Response of tropical atmosphere to local, steady forcing. *Mon. Wea. Rev.,* **100,** 518–541.

——, 1983: Mechanisms of monsoon low-frequency variability—Surface hydrological effects. *J. Atmos. Sci.,* **40,** 2110–2124.

——, 1994: The role of hydrological processes in ocean-atmosphere interactions. *Rev. Geophys.,* **32,** 427–476.

——, and L. C. Chou, 1980: Low-frequency transitions of a simple monsoon system. *J. Atmos. Sci.,* **37,** 368–382.

——, and C. D. Hoyos, 2004: Prediction of the monsoon rainfall and river discharge on 15–30-day time scales. *Bull. Amer. Meteor. Soc.,* **85,** 1555–1572.

——, V. O. Magana, T. N. Palmer, J. Shukla, R. A. Tomas, M. Yanai, and T. Yasunari, 1998: Monsoons: Processes, predictability,

and the prospects for prediction. *J. Geophys. Res.,* **103** (C7), 14 451–14 510.

——, A. M. Moore, J. P. Loschnigg, and R. R. Leben, 1999: Coupled ocean-atmosphere dynamics in the Indian Ocean during 1997-98. *Nature,* **401,** 356–360.

Xie, S. P., H. M. Xu, N. H. Saji, Y. Q. Wang, and W. T. Liu, 2006: Role of narrow mountains in large-scale organization of Asian monsoon convection. *J. Climate,* **19,** 3420–3429.

Yanai, M., S. Esbensen, and J. H. Chu, 1973: Determination of bulk properties of tropical cloud clusters from large-scale heat and moisture budgets. *J. Atmos. Sci.,* **30,** 611–627.

——, B. Chen, and W. W. Tung, 2000: The Madden–Julian oscillation observed during the TOGA COARE IOP: Global view. *J. Atmos. Sci.,* **57,** 2374–2396.

Yang, S., W. S. Olson, J. J. Wang, T. L. Bell, E. A. Smith, and C. D. Kummerow, 2006: Precipitation and latent heating distributions from satellite passive microwave radiometry. Part II: Evaluation of estimates using independent data. *J. Appl. Meteor. Climatol.,* **45,** 721–739.

Yasunari, T., 1979: Cloudiness fluctuations associated with the Northern Hemisphere summer monsoon. *J. Meteor. Soc. Japan,* **57,** 227–242.

Zhang, C., 2005: Madden-Julian oscillation. *Rev. Geophys.,* **43,** RG2003, doi:10.1029/2004RG000158.

Zuidema, P., and B. E. Mapes, 2008: Cloud vertical structure observed from space and ship over the Bay of Bengal and eastern tropical Pacific. *J. Meteor. Soc. Japan,* **86A,** 205–218.